energies

MDPI

Article

A Novel Harris-Hawk-Optimization-Based Maximum-Power-Point-Tracking Control Strategy for a Grid-Connected PV Power-Generation System

Xiang Tao [1], Jianbo Xin [1], Shuai Zhang [2,*], Zaide Xu [1], Zhonghai Ye [3], Kai Wang [3], Bo Chen [1] and Ning Zhou [1]

[1] State Grid Jiangxi Electric Power Research Institute, Nanchang 330096, China; xiangtao358@gmail.com (X.T.); mandyzhuhai@163.com (J.X.); jxdky_xuzaide@126.com (Z.X.); orchis1986@126.com (B.C.); zhouning1982@163.com (N.Z.)
[2] School of Control Science and Engineering, Shangdong University, Jinan 250100, China
[3] State Grid Jiangxi Electric Power Company Limited, Nanchang 330096, China; yezhonghai1@126.com (Z.Y.); wangkwh@163.com (K.W.)
* Correspondence: spritstronger@126.com

Abstract: This paper aims to assess the efficacy of the Harris Hawk Optimization (HHO) algorithm within the domain of photovoltaic (PV) power-generation systems. The focus lies in elucidating how the HHO algorithm optimizes maximum-power-point tracking (MPPT) and augments the performance of grid-connected PV systems. Initially, in the MATLAB/Simulink environment, a comparison is made between the HHO algorithm and two other extensively utilized methods for maximum-power-point tracking (MPPT): Perturb and Observe (P&O) and Particle Swarm Optimization (PSO). Preliminary findings indicate the HHO algorithm's notable advantages in efficiency and speed over the other algorithms. Furthermore, by establishing a practical experimental platform and synchronously verifying outcomes through simulation, we conducted a comprehensive assessment of the HHO algorithm on a single-phase full-bridge-inverter grid-connected system. Results show the HHO algorithm's exceptional optimization capabilities, which displays superior adaptability and ability to adjust to varying external conditions.

Keywords: PV power-generation system; MPPT; Harris Hawk Optimization; grid-connected control strategy

Citation: Tao, X.; Xin, J.; Zhang, S.; Xu, Z.; Ye, Z.; Wang, K.; Chen, B.; Zhou, N. A Novel Harris-Hawk-Optimization-Based Maximum-Power-Point-Tracking Control Strategy for a Grid-Connected PV Power-Generation System. *Energies* **2024**, *17*, 76. https://doi.org/10.3390/en17010076

Academic Editor: Abdelali El Aroudi

Received: 13 November 2023
Revised: 17 December 2023
Accepted: 20 December 2023
Published: 22 December 2023

1. Introduction

With the development of the world economy, the global energy challenge has become increasingly prominent. In response, clean and reliable solar power generation has garnered significant attention from scholars and has emerged as the preferred choice for many countries. Its advantages, including easy accessibility, abundant reserves, and environmental friendliness, have contributed to its growing prominence. As the production cost of PV modules continues to decrease and the conversion efficiency of solar cells improves, PV power generation is gradually taking on a more significant role, transitioning from being a supplementary energy source to a primary alternative energy solution in various domains [1].

In the pursuit to enhance the efficiency of PV power generation, both domestic and foreign scholars have conducted extensive research on maximum-power-point tracking (MPPT). The disturbance observation method [2], a traditional control approach, has gained widespread adoption due to its simplicity and ease of implementation. However, it often falls short in terms of speed and steady-state accuracy, and the system may occasionally misjudge the maximum-power point. A novel approach was introduced in [3], known as the jump adaptive-disturbance-observation method. This method exhibits rapid responsiveness to environmental variations and effectively mitigates system disturbances

when operating at the maximum-power point. In [4], a variable step-size perturbation and observation method was devised. This method incorporates a step-size adjustment strategy, where if the product of the two differences, namely the output-power difference and the voltage difference before and after perturbation is found to be negative, the perturbation step size is halved from its initial value, and the direction of the perturbation is changed accordingly. Similar methods include conductance increment methods [5], which are based on traditional single-peak mathematical characterization, but these cannot cope with non-convex function optimization problems in a non-uniform irradiance.

In order to find the maximum-power points in the multi-peak characteristics of PV arrays, various intelligent algorithms have been proposed, such as the improved Team Game Optimization algorithm (ITGO) [6], the improved Social Ski Driver algorithm (ISSD) [7], the Hierarchical Pigeon-excitation Optimization algorithm (HPIO) [8], and the modified Butterfly Optimization algorithm (MBO) [9] et al. By introducing random factors and improving their global search ability, these algorithms can be applied to a variety of nonlinear and non-convex complex optimization problems.

Particle swarm optimization (PSO) has emerged as a hot research area in recent years, offering better speed and steady-state accuracy compared with traditional control algorithms. However, PSO is sensitive to the initial position and exhibits poor stability, and this results in significant fluctuations in voltage and power, leading to low energy utilization. To enhance the efficiency and convergence speed of the Particle Swarm Optimization (PSO) algorithm, the proper initialization of particles is crucial to finding the optimal solution. In [10], the author proposed a two-stage algorithm to address this issue. In the first stage, the Perturb and Observe (P&O) method is utilized to determine the nearest local maximum, followed by the second stage, where the PSO method is employed to achieve global peak (GP) optimization. However, it was observed that the P&O technique takes longer to determine the maximum-power point (MPP). To address this limitation, the authors in [11] made improvements by removing the randomization of the standard PSO acceleration factor. This modification aims to reduce the search time. Nonetheless, it is necessary to limit the change in particle velocity since low-velocity values may require more iterations to reach the GP, while excessively large velocity values could lead to escaping the GP. Striking the right balance in the particle-velocity adjustment becomes crucial for the success of the optimization process. In addition, an improved Salp Swarm algorithm [12] improves the global search capability by adding Pareto distribution and chaotic mapping to the leader-position update process and introduces a discrepancy strategy to improve the local search process. Artificial neural networks [13] have also been used to predict the range in which the maximum-power point lies, and a simple feedforward neural network can estimate the domain in which the maximum-power point lies based on the variation in temperature and irradiance. In [14], a self-tuning scheme based on reinforcement learning was proposed, which can improve the convergence speed and introduce β parameter, which has been proven to track the MPP more efficiently, to make a constrained search space to obtain higher MPPT performance.

Although so many metaheuristic algorithms have been used to solve the multi-peak problem, the various algorithms have their own advantages and disadvantages in terms of tracking accuracy and tracking speed. Selecting an MPPT algorithm with higher tracking accuracy and faster tracking speed is important for optimizing the PV power output. In partial shading conditions, the P-V curve of a photovoltaic array often shows multiple peaks. Traditional algorithms tend to prioritize local searches during optimization, which results in becoming stuck in the local optima. Conversely, HHO, inclined to explore the search space, readily avoids the local optima, thereby aiding in locating the maximum-power point.

For higher tracking accuracy and faster tracking speeds, this paper incorporates the Harris Hawk Optimization algorithm [15] to create a new MPPT control strategy. In order to verify its effectiveness, the P&O and PSO methods are used for MATLAB/Simulink (version R2021a) simulations. By analyzing the convergence characteristic curves of the output power, output voltage, and duty cycle, the feasibility and effectiveness of the proposed HHO algorithm can be evaluated. Additionally, this paper analyzes and summarizes the topology of a grid-connected inverter. After considering switching loss and control difficulty, the single-phase full-bridge-inverter circuit is selected as the scheme for the grid-connected PV power-generation simulation system. To simulate potential local shading issues in real-world scenarios, the output characteristics of the PV panels are modified, causing irradiance changes during the simulation for 1 s.

2. Modeling and Analysis of the PV Cell

2.1. Mathematical Model

From Kirchhoff's law of voltage, the Kirchhoff's law of current can be obtained:

$$I = I_{ph} - I_0\left(e^{\frac{q(U+IR_s)}{AKT}} - 1\right) - \frac{U + IR_s}{R_p} \tag{1}$$

Equation (1) is the mathematical expression [16] of the output current of PV cells, and the meaning of each parameter in the equation is shown in Table 1.

Table 1. Parameter representation of the solar-cell model.

Parameters	Meaning
I	Output current
U	Output voltage
I_{ph}	Photocurrent
R_s	Series resistance
R_p	Shunt resistance
I_0	Diode reverse saturation current
q	Electronic charge; 1.6×10^{-19} C
K	Boltzmann constant; 1.3×10^{-28} J/K
A	Diode curve factor; usually 1
T	Absolute temperature

2.2. Engineering Model

The mathematical model parameters expressed by Equation (1) are numerous, and determining many of these parameter values can be challenging. As a result, accurately solving the model becomes very difficult, making it impractical for engineering applications. To address this issue, a reasonable simplification can be applied to obtain an engineering model for PV cells. The engineering model of the output characteristics of PV cells under general working conditions can be expressed as

$$\begin{cases} I_{sc} = I_{sc}\frac{S}{S_{ref}}(1 + a\Delta T) \\ U_{oc} = U_{oc}(1 - c\Delta T)\ln(1 + b\Delta S) \\ I_m = I_m\frac{S}{S_{ref}}(1 + a\Delta T) \\ U_m = U_m(1 + c\Delta T)\ln(1 + b\Delta S) \end{cases} \tag{2}$$

The formula includes parameters such as I_{sc}, I_m, U_m, and U_{oc}, which, respectively, represent the short-circuit current, maximum-power-point current, maximum-power-point voltage, and open-circuit voltage under standard conditions. These standard conditions entail a reference solar-radiation intensity of 1000 W/m^2 and a reference battery temperature of 25 °C [17]. Additionally, ΔT and ΔS denote the temperature difference and relative irradiance between general working conditions and the standard conditions. Utilizing the above model, it becomes feasible to calculate the output characteristics under normal working conditions.

3. The HHO-Based MPPT Algorithm

The Harris Hawk Optimization (HHO) algorithm is an innovative swarm bionic intelligence approach inspired by the predatory behavior of Harris hawks. At the core of this algorithm is the concept of the cooperative predation behavior among hawks. A group of Harris hawks surprises their prey by attacking from different directions, mirroring the hunting model observed in Harris hawks. The hawks work in coordination during the attack, while the leader of the Harris hawks strikes the target prey, stalks it, and suddenly moves out of sight, allowing the next Harris hawks to continue the pursuit. This tactical strategy effectively wears down the prey, eventually leading to its capture. The HHO algorithm demonstrates superior applicability to constraint problems compared with other algorithms. Additionally, as a global optimization method, HHO maintains a well-balanced trade-off between the development phase and the exploration phase. The HHO algorithm primarily consists of three main phases: the exploration phase, the transition phase from exploration to development, and the development phase.

3.1. Exploration Phase

Harris hawks roost somewhere randomly and search for prey through one of two strategies, with the random number q used to select the strategy to be employed.

$$\begin{cases} X(t+1) = \begin{cases} X_{rand}(t) - r_1|X_{rand}(t) - 2r_2X(t)|, q \geq 0.5 \\ (X_{rabbit}(t) - X_m(t)) - r_3(LB + r_4(UB - LB)), q < 0.5 \end{cases} \\ X_m(t) = \frac{1}{N}\sum_{i=1}^{N} X_i(t) \end{cases} \tag{3}$$

where $X(t)$ represents the current position of the Harris hawk; $X_{rabbit}(t)$ represents the position of the prey rabbit; r_1, r_2, r_3, and r_4 are random numbers between 0 and 1; UB and UL indicate the position range of the hawk, which is determined by the range of the independent variable of the optimization function; $X_m(t)$represents the average position of the hawk; and N is the total number of hawks.

3.2. Transition Phase

HHO can switch between different exploitation behaviors according to the escape energy of the prey, and the prey energy will be greatly reduced in the process of escape. The prey energy can be expressed as

$$E = 2E_0\left(1 - \frac{t}{T}\right) \tag{4}$$

where E is the escape energy of the prey, E_0 is the initial energy of the prey, t is the current iteration, and T is the maximum iteration. In this phase, when $E \geq 0.5$, a soft siege is launched; when $E < 0.5$, a hard siege is initiated.

3.3. Development Phase

(1) Soft siege

When $r \geq 0.5$ and $|E| \geq 0.5$, the following model is adopted:

$$X(t+1) = \Delta X(t) - E|JX_{rabbit}(t) - X(t)| \tag{5}$$

where $\Delta X(t) = X_{rabbit}(t) - X(t)$ is the distance between the prey and the hawks, J is a random number between 0 and 2.

(2) Hard siege

When $r \geq 0.5$ and $|E| < 0.5$, the following model is adopted:

$$X(t+1) = X_{rabbit}(t) - E|\Delta X(t)| \tag{6}$$

(3) Progressive fast-dive soft siege

When $r < 0.5$ and $|E| \geq 0.5$, the prey can still escape successfully, so the raid will still be preceded by a soft siege, which will use the following strategy to update the position:

$$\begin{array}{l} X(t+1) = \begin{cases} Y, F(Y) < F(X(t)) \\ Z, F(Z) < F(X(t)) \end{cases} \\ Y = X_{rabbit}(t) - E|JX_{rabbit}(t) - X(t)| \\ Z = Y + S \times LF(D) \end{array} \tag{7}$$

where D and S are the dimensions of the objective function and the random vector, respectively, and LF is the mathematical expression of Levy's flight.

(4) Progressive fast-dive hard siege

When $r < 0.5$ and $|E| < 0.5$, this strategy is adopted:

$$X(t+1) = \begin{cases} Y, F(Y) < F(X(t)) \\ Z, F(Z) < F(X(t)) \end{cases} \tag{8}$$

where Y and Z are calculated as follows:

$$\begin{cases} Y = X_{rabbit}(t) - E|JX_{rabbit}(t) - X_m(t)| \\ Z = Y + S \times LF(D) \end{cases} \tag{9}$$

3.4. Objective Fitness Function

For the MPPT control design, the output power of the photovoltaic array is commonly used as the fitness function, with the duty cycle D as the independent variable of the fitness function. The fitness function is defined as follows:

$$P_k(D_k) = U_k I_k \tag{10}$$

where k represents the iteration number, D_k indicating the duty cycle used during the k-th iteration, U_k and I_k represents the obtained output voltage and current.

The MPPT control flow chart of the HHO algorithm is shown in Figure 1.

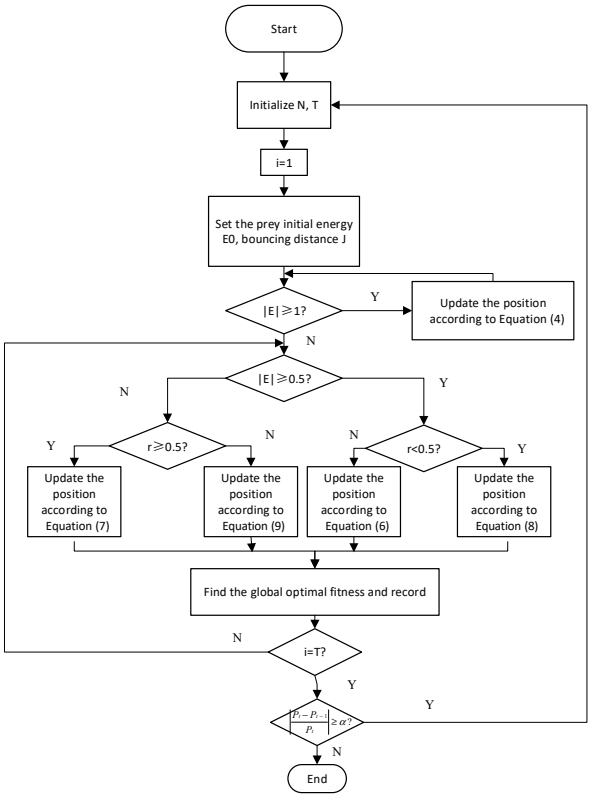

Figure 1. Control flow chart of HHO.

4. Simulation Analysis and Verification

4.1. MPPT Control System Based on a Boost Converter

In the study's PV system design, the PV array's output voltage is low, only reaching tens of volts. Considering the relatively low output voltage of the PV arrays, the Boost circuit is a suitable choice. Additionally, the output characteristics of the Boost circuit are superior to those of Buck-Boost, and it imposes lower demands on the output voltage filtering. Therefore, the Boost circuit is chosen as the topology for the DC/DC conversion circuit in the PV system.

The simulation model selects a single PV array as the tracking object. The PV panel parameters and the Boost design parameters are shown in Tables 2 and 3.

Table 2. PV panel parameters.

Variable	Description	Units	Numerical Value
V_{oc}	Open-circuit voltage	V	36.3
I_{sc}	Short-circuit current	A	7.84
P_m	Peak power	W	213.15
I_m	Peak-power-point current	A	7.35
V_m	Peak-power-point voltage	V	29

Table 3. Boost circuit parameters.

Variable	Description	Units	Numerical Value
L_1	Input inductance	mH	1
C_2	Output capacitance	μF	2200
R_L	Load resistance	Ω	20
f_s	Switching frequency	kHz	20

PSO, P&O, and HHO algorithms are respectively used in the established Simulink simulation model to compare and analyze their speediness, stability, and so on. The power and duty cycle curves of three different algorithms (red represents the output power P(W) of PV panels; green represents the duty cycle D) are as shown in Figure 2. Due to HHO's inclination toward exploring the search space more extensively than PSO, employing the HHO algorithm results in greater power fluctuations.

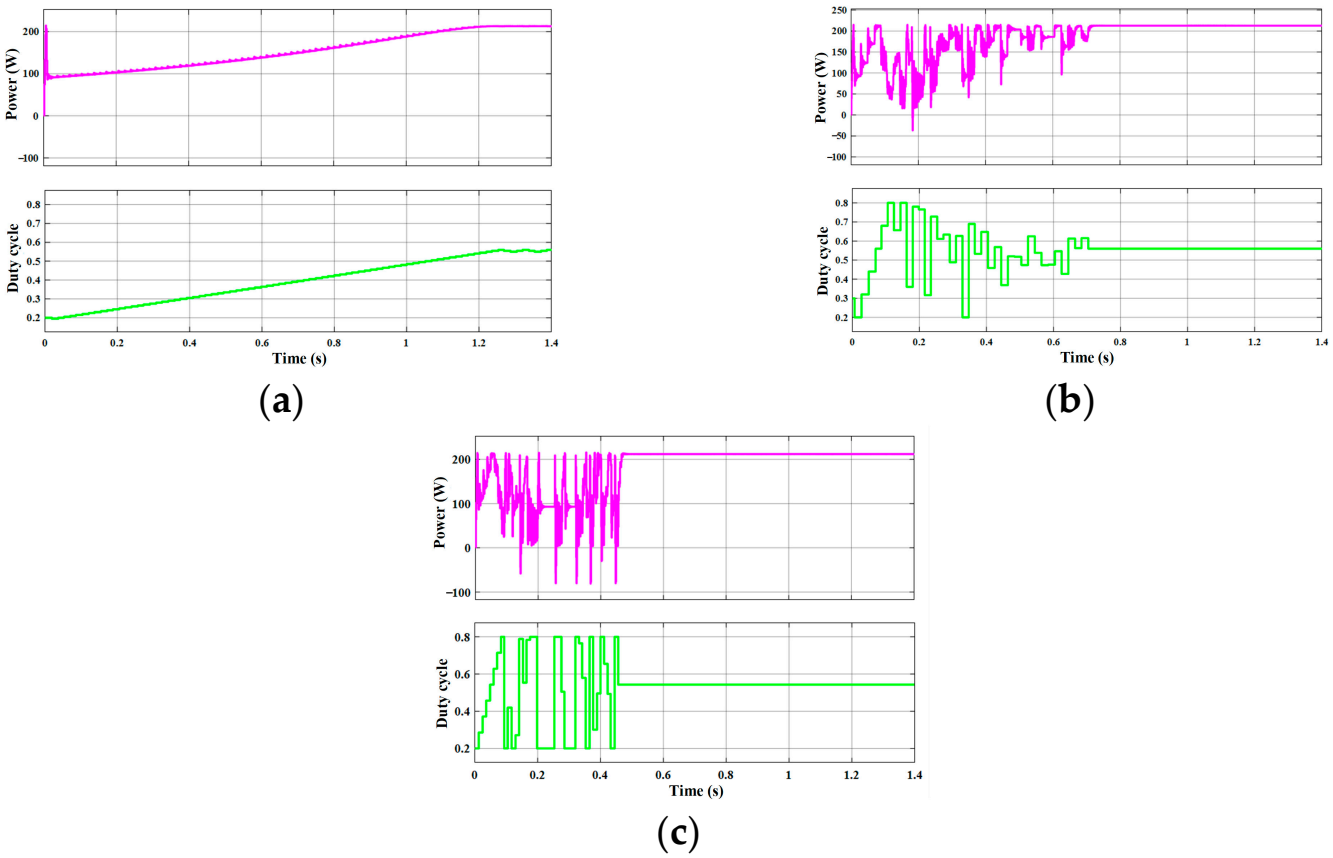

Figure 2. Power and duty cycle curves obtained by the (**a**) P&O algorithm, (**b**) PSO algorithm, and (**c**) HHO algorithm, respectively.

The time taken by each algorithm to find the maximum-power point and the corresponding duty cycle and output power are summarized in Table 4.

Table 4. Comparison of the effects of the three algorithms.

Algorithms	Convergence Time (s)	Duty Cycle	Power Output (W)
P&O	1.25	0.56	211.0
PSO	0.73	0.55	212.7
HHO	0.45	0.57	213.1

Based on the above simulation results, all three algorithms, namely PSO, P&O, and HHO, successfully identify the maximum-power point and operate stably with a corresponding duty cycle of approximately 0.56. Under this duty cycle, the output power of the PV panel reaches close to the maximum-power value of 231.15 W.

However, due to the distinct optimization methods employed by each algorithm, their speediness and stability vary. The control scheme based on the HHO algorithm demonstrates exceptional performance, taking only 0.45 s to find the maximum-power point and maintain stability. The PSO algorithm is slightly slower, requiring 0.73 s, but still achieves satisfactory stability. On the other hand, the P&O algorithm exhibits a longer

computation time and, at times, exhibits small oscillations near the maximum-power point. Such oscillations can hinder a stable system operation. The P&O algorithm's continuous disturbance results in constant changes in the system's operating point, leading to an unstable state near the oscillation point rather than working stably at the exact maximum-power point. In contrast, the PSO algorithm employs a random search and constantly updates the optimal value, with all particles approaching the optimal value. As seen in the duty-cycle curve, the duty cycle converges slowly to the best value, eventually achieving stable operation at the found maximum-power point without the oscillation phenomenon observed in P&O. Meanwhile, the convergence speed of the PSO algorithm heavily relies on the proper selection of the initial values. Poor initial values may lead to slow convergence or even prevent the algorithm from finding the optimal value within the set number of iterations. On the other hand, the HHO algorithm's higher intelligence allows it to adaptively search through a series of comparison changes, utilizing distinct search strategies for various scenarios. Consequently, its speediness surpasses that of the other two algorithms and remains unaffected by the initial position. In conclusion, the HHO algorithm demonstrates both speed in finding the maximum-power point and outstanding stability in its operational state, thereby verifying its effectiveness and reliability.

4.2. Experimental Verification

The simulation results confirm the feasibility of the algorithm proposed in this paper. To further validate the practical effectiveness of the algorithm, an experimental platform for the photovoltaic power-generation MPPT control system was constructed. The platform mainly consists of the following components: a photovoltaic simulator, an MPPT controller based on the STM32F103ZET6 microcontroller, a self-made Boost converter, auxiliary power modules, current–voltage sampling modules, and a 20 Ω load resistor. The experimental platform is illustrated in Figure 3.

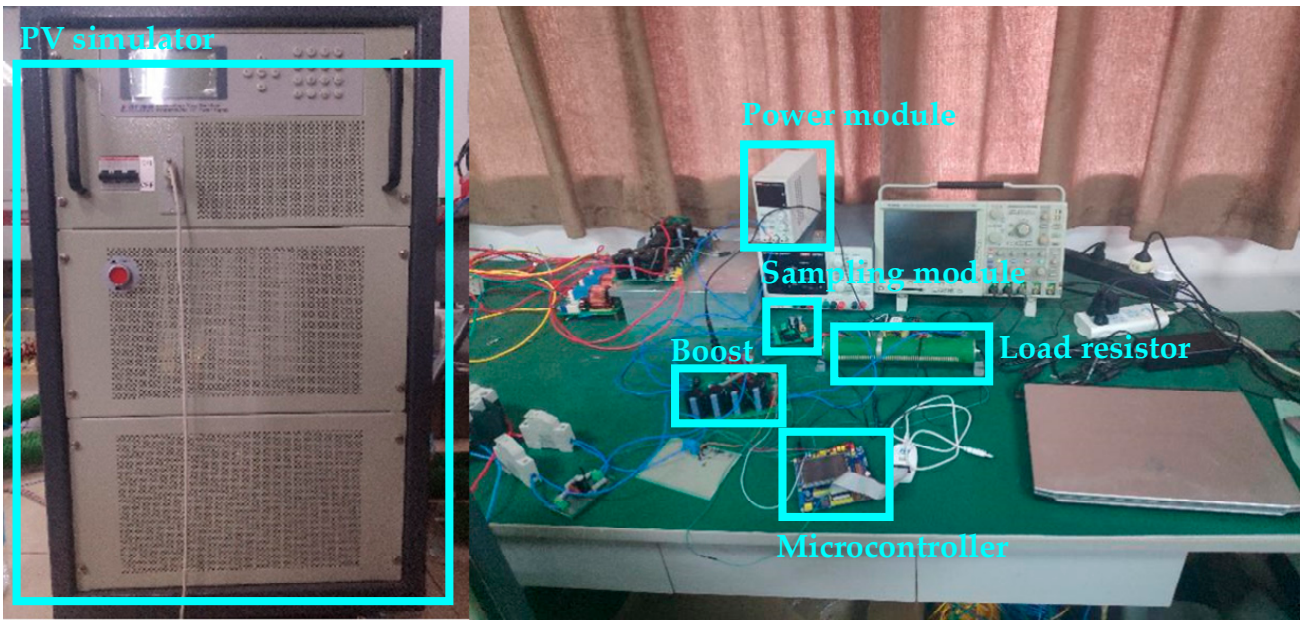

Figure 3. Photovoltaic power-generation MPPT control system experimental platform.

The photovoltaic simulator can generate characteristic curves of the individual photovoltaic cell output by setting the short-circuit current and open-circuit voltage to simulate an actual photovoltaic array. Setting the open-circuit voltage (V_{oc}) of the photovoltaic simulator to 30 V and the short-circuit current (I_{sc}) to 3.0 A generates a maximum-power-point voltage (V_{mpp}) of 21.0 V, a maximum-power-point current (I_{mpp}) of 2.4 A, and a maximum power (P_{mpp}) of 49.80 W. Due to certain deviations between the simulator's actual output and the generated output, for more realistic and reliable results, actual output parameters were selected for computation. The actual output is V_{mpp} = 25.4 V, I_{mpp} = 2.4 A, and P_{mpp} = 60.96 W.

Building upon the aforementioned experimental platform, tests were conducted on three different algorithms—P&O, PSO, and HHO. An oscilloscope and photovoltaic simulator control software were used to record the output voltage, power, changes in the duty cycle of the switches, and the optimal operating point obtained from the experiments. Figures 4–6 present the experimental results for the P&O, PSO, and HHO, respectively.

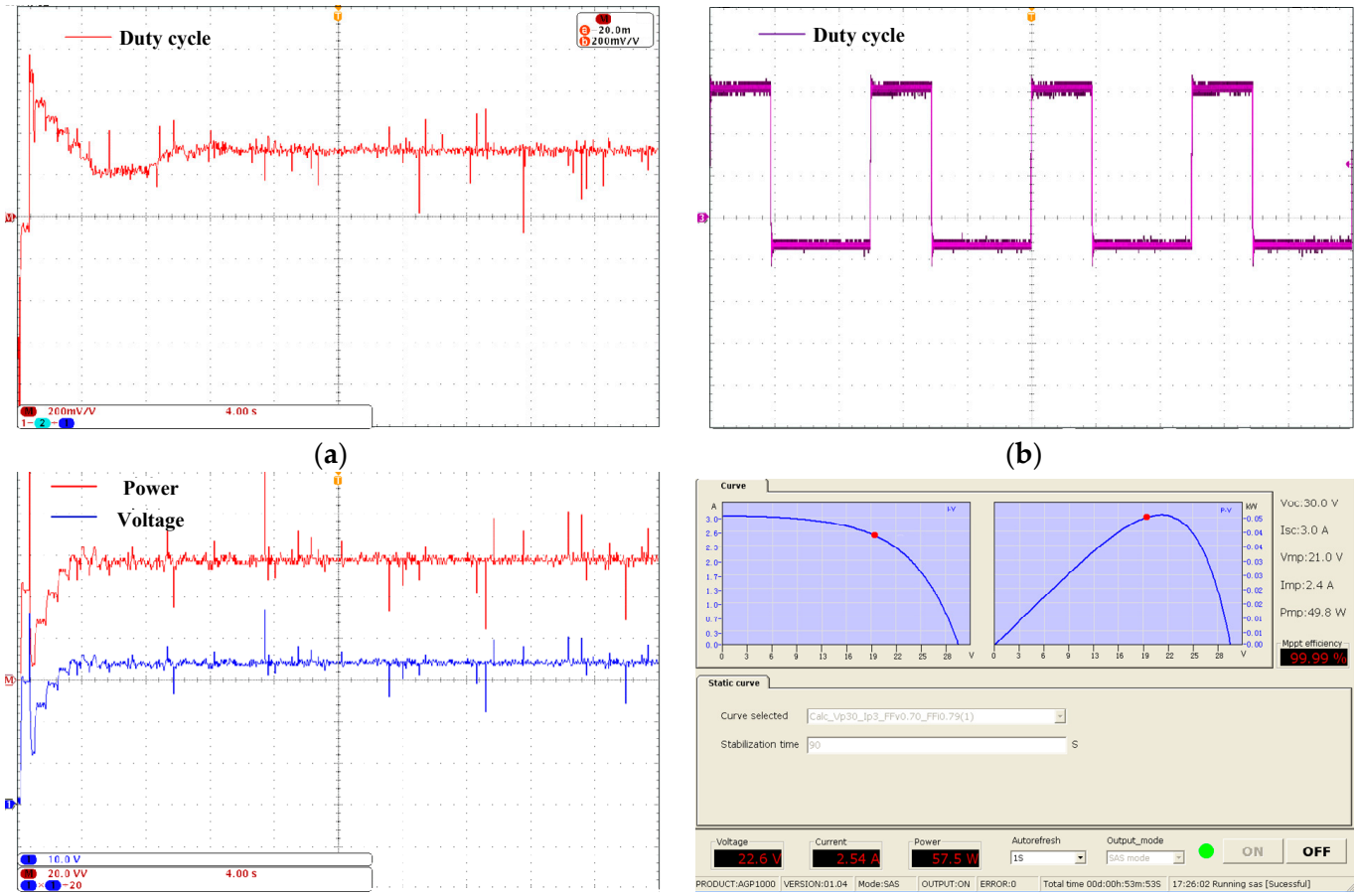

Figure 4. Experiment results of P&O. (**a**) Duty-cycle curve; (**b**) Duty-cycle curve at stable operation; (**c**) Output power and voltage curves; (**d**) Optimal operating point.

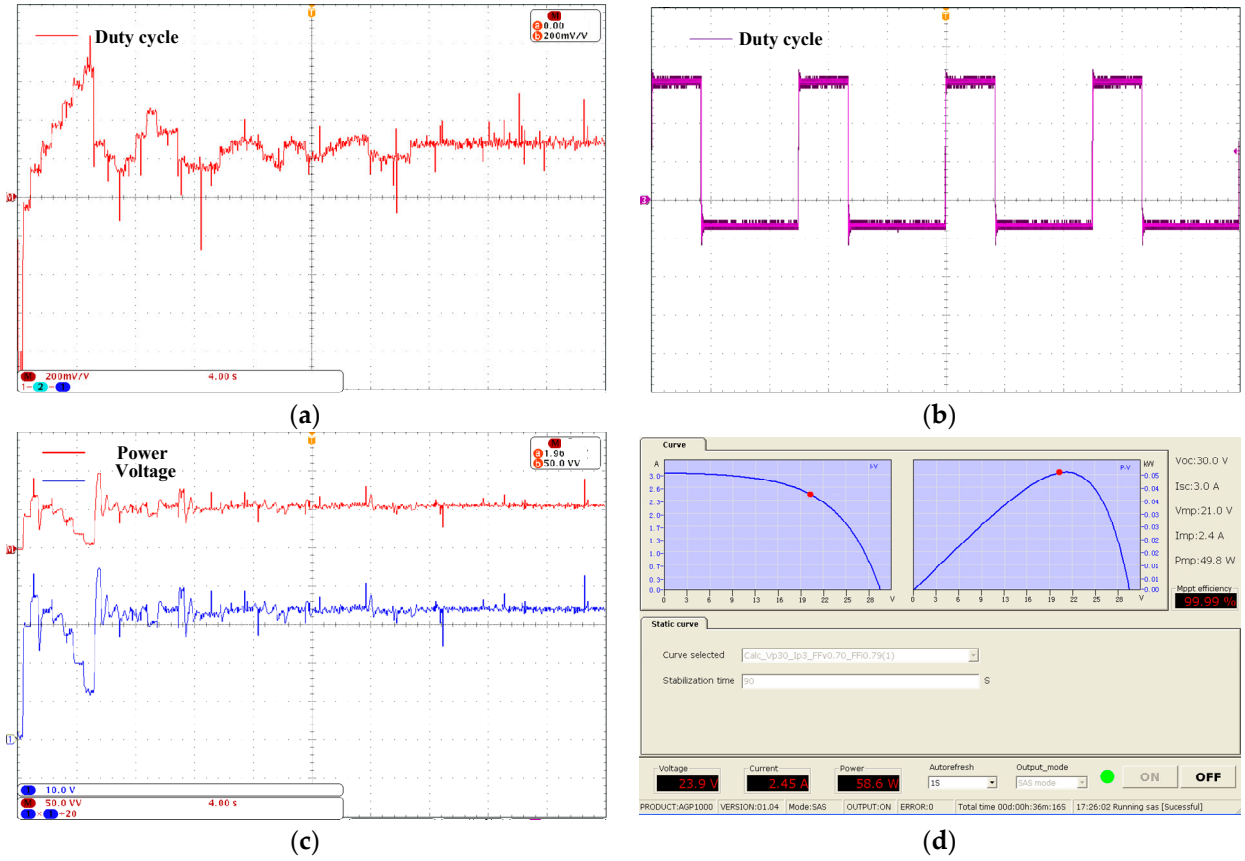

Figure 5. Experiment results of PSO. (**a**) Duty-cycle curve; (**b**) Duty-cycle curve at stable operation; (**c**) Output power and voltage curves; (**d**) Optimal operating point.

The operational effectiveness of the three MPPT algorithms is depicted in Table 5.

Table 5. Experimental results of the three MPPT algorithms.

Algorithms	P_{max}/W	P_o/W	Tracking Time	System Efficiency
P&O	60.96	57.5	1.2 s	94.3%
PSO	60.96	58.6	2.8 s	96.1%
HHO	60.96	59.7	1.6 s	97.9%

Under the set operating conditions, all three algorithms—P&O, PSO, and HHO—achieved maximum-power-point tracking. The output duty cycles for P&O, PSO, and HHO were 0.380, 0.340, and 0.311, respectively. The proposed HHO algorithm in this study demonstrated promising results during experimentation, yielding an output power of 59.7 W with an impressive efficiency of 97.9%. This efficiency surpasses that of the other two algorithms. Additionally, the HHO algorithm tracked the maximum-power point in a swift 1.6 s, outperforming the PSO algorithm in tracking time. In contrast, the P&O algorithm, while exhibiting faster tracking, presented an efficiency of only 94.3%. Furthermore, the P&O algorithm tends to oscillate near the maximum-power point, potentially causing the system's operating point to deviate and even leading to an unstable system state.

In summary, the proposed HHO algorithm in this paper demonstrates a certain advantage in terms of both speed and stability compared with other algorithms.

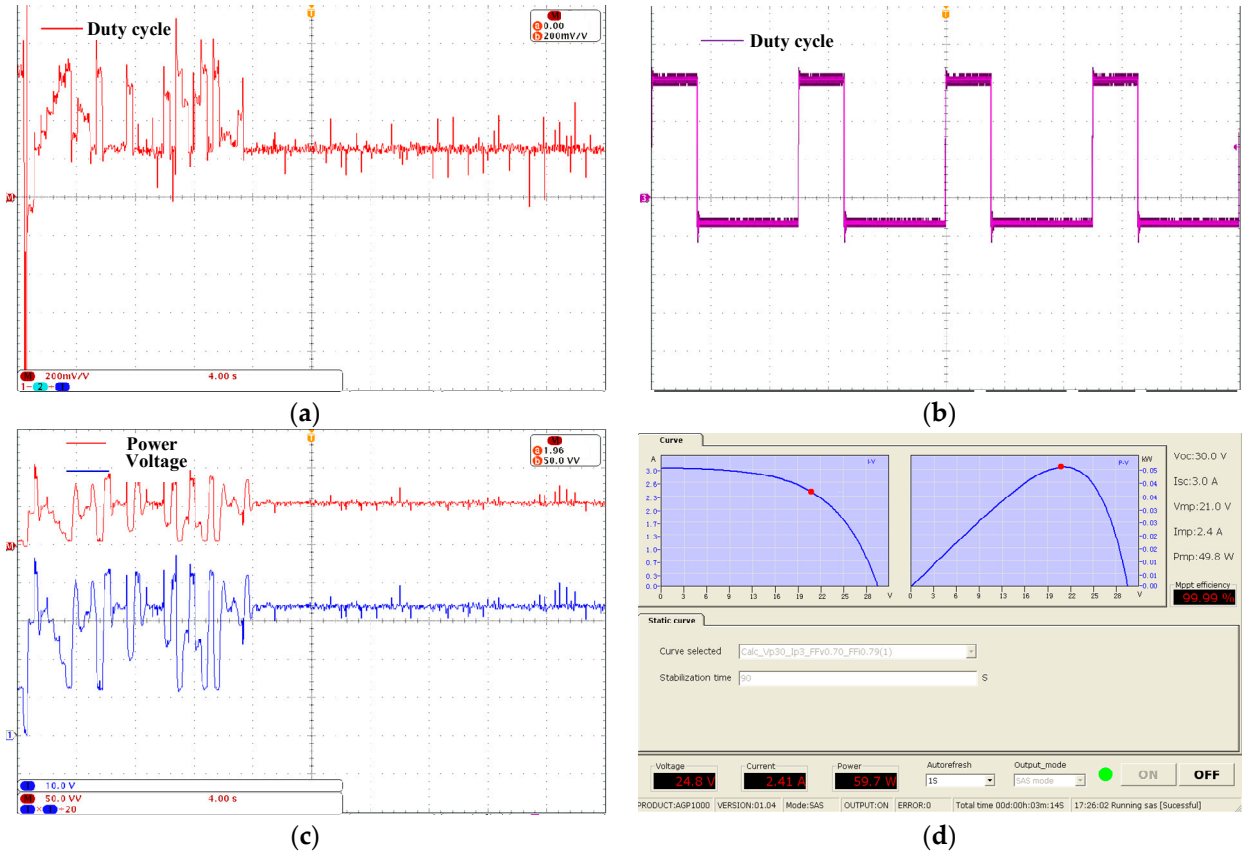

Figure 6. Experiment results of HHO. (**a**) Duty cycle curve; (**b**) Duty cycle curve at stable operation; (**c**) Output power and voltage curves, (**d**) Optimal operating point.

5. The HHO-Based MPPT Control for a Grid-Connected PV Power-Generation System

5.1. Design of the Grid-Connected PV Inverter

To better simulate real-world application scenarios, the PV power-generation system studied in this paper adopts a single-phase full-bridge-voltage-type active inverter circuit [18].

After the Boost converter, the output DC voltage from the PV array is increased to a higher level. This DC voltage is then converted into 220 V AC power by the inverter. Finally, the AC power is filtered through an inductor and connected to the grid. The use of the single-phase full-bridge-voltage-type active inverter circuit allows for efficient conversion of the DC power from the PV array into usable AC power, facilitating its integration with the grid for practical energy utilization.

5.2. Structure of the Grid-Connected PV Power-Generation System

On the foundation of the maximum-power-point tracking circuit for a single PV array, the load resistance is replaced by a single-phase bridge inverter. The PV array and the DC/DC conversion circuit controlled by MPPT are represented by an equivalent DC power supply, as shown in Figure 7. The DC power is then converted into a 220 V power frequency alternating current through a single-phase full-bridge inverter circuit with inductive filtering. The double closed-loop control system takes the output current of the inverter, DC voltage, and grid voltage as input, and produces the pulse-width control signal for the switching tubes as output. To minimize steady-state error and enhance the

anti-interference capability, a PI controller with a low-pass filter is employed. The transfer function of the controller is as follows:

$$G_{cv}(s) = \frac{\tau_1 s + 1}{\tau_0 s(\tau_2 s + 1)} \tag{11}$$

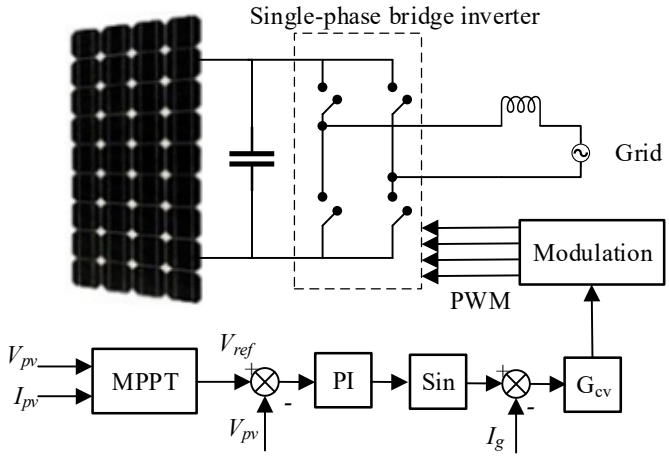

Figure 7. PV power-generation grid-connected system.

The control parameters are determined by the following formula:

$$\begin{cases} \tau_1 = \frac{1}{2\pi f_{cv}} \sqrt{\frac{1+\sin\gamma}{1-\sin\gamma}} \\ \tau_2 = \frac{1}{2\pi f_{cv}} \sqrt{\frac{1-\sin\gamma}{1+\sin\gamma}} \\ \tau_0 = \frac{\tau_1}{2\pi C f_{cv}} \end{cases} \tag{12}$$

where f_{cv} is the voltage-loop open-loop cutoff frequency and γ is the phase-angle margin of the system. The PI controller parameters are calculated as $\tau_1 = 3.08 \times 10^{-2}$, $\tau_2 = 3.65 \times 10^{-3}$, and $\tau_0 = 1.63 \times 10^{-1}$.

5.3. Simulation Analysis

In order to simulate changes in external conditions during actual operation, such as variations in irradiance caused by local shading of PV panels, two PV panels are connected in series [19]. At the simulation time of 1 s, the irradiance of one array is reduced from 1000 W/m^2 to 600 W/m^2. When the two PV arrays are connected in series, the maximum output power P_{max} is 1002.2 W. With the reduction in irradiance to 600 W/m^2, the maximum power decreases to 305.3 W. Therefore, the theoretical maximum output power of the two series-connected PV arrays is P_{max}' = 806.4 W.

5.3.1. Output Voltage and Current of Inverter

The output voltage and current of inverter waveforms using the three different algorithms are shown in Figure 8. The horizontal axis of the coordinate diagram represents time, while the vertical axis represents the amplitude. The black curve represents the output voltage, which is approximately constant and reduced 20-fold for easier observation. The blue curve represents the output current. By analyzing the phase relationship between the two curves, it can be determined whether the grid connection is successful [20]. When the two curves are in phase, it indicates that the grid connection is successful.

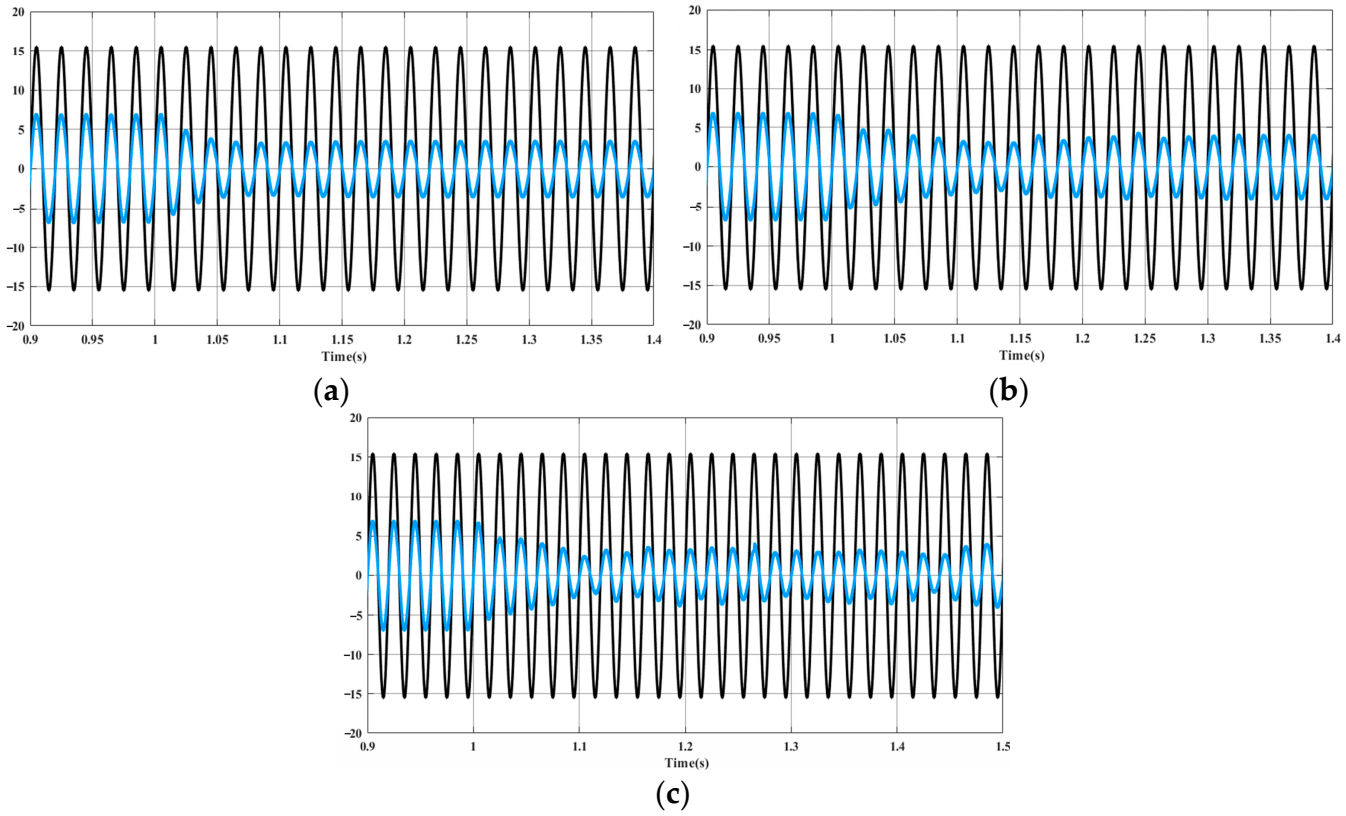

Figure 8. Output voltage and current waveforms of the inverter using (**a**) P&O, (**b**) PSO, and (**c**) HHO.

Before the change in irradiance, each algorithm successfully tracked the maximum-power point and connected to the grid. However, as the irradiance decreases, the output power of inverter also decreases. After the irradiance changes, the three algorithms restart and find new operating points. The output-current amplitude of the P&O, PSO, and HHO algorithms decreases from 6.0 A before the irradiance change to 3.5 A, 4.0 A, and 4.25 A, respectively. Among them, the performance of the P&O algorithm in the presence of uneven lighting on the PV array is the worst. The basic principle of the P&O algorithm makes it prone to becoming stuck in the local optima when dealing with multi-peak optimization problems. As the PV array experiences local shading, its P-V curve also exhibits multi-peak characteristics. On the other hand, the PSO algorithm has intelligent search capabilities and is more likely to find the global optima compared with the P&O algorithm. However, the speed of the search is highly dependent on the initial position and parameters of the position and velocity-update formula. In contrast, the HHO algorithm demonstrates superior performance. It can quickly find the global optimum without the need to set as many parameters as required by the PSO algorithm. Overall, the HHO algorithm proves to be efficient and effective at handling changes in irradiance and optimizing the PV system's performance.

5.3.2. The Change in Output Power and Duty Cycle before and after the Change in Irradiance

The power and duty-cycle change curves of the three algorithms before and after the irradiance change are shown in Figure 9.

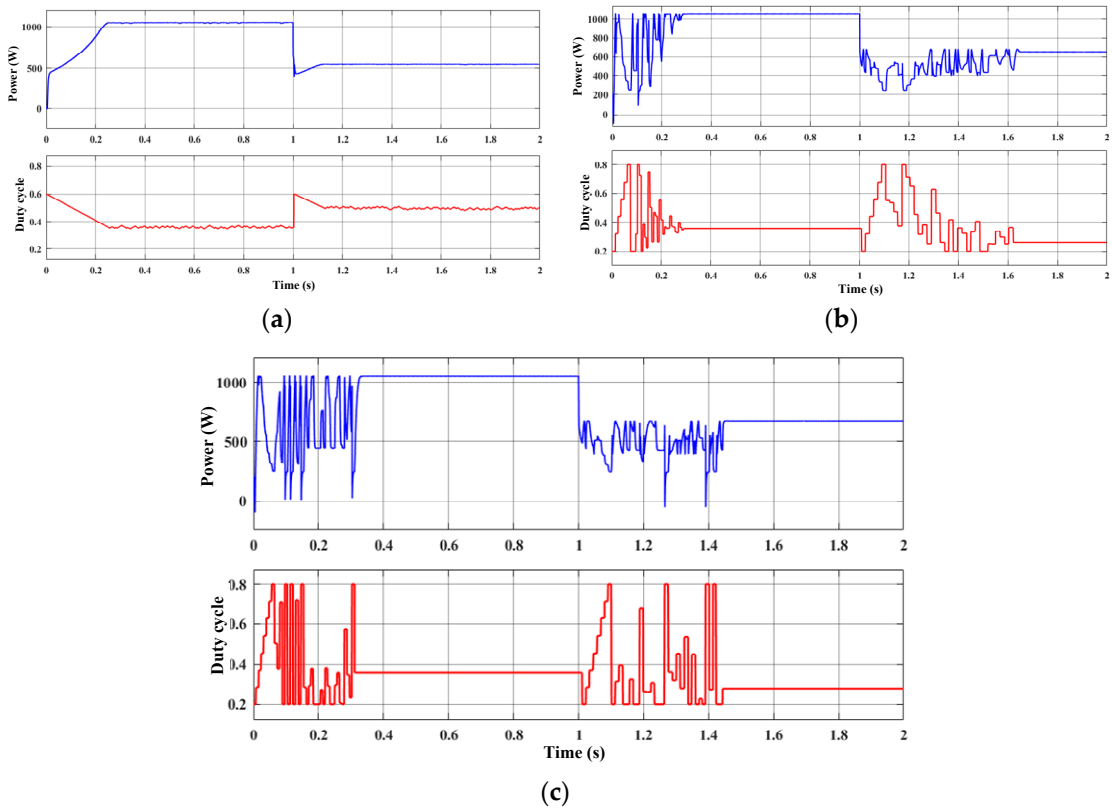

Figure 9. The power and duty-cycle change curves of (**a**) P&O, (**b**) PSO, and (**c**) HHO algorithms before and after the irradiance change.

The simulation results demonstrate that all three algorithms are capable of achieving maximum-power tracking. However, there are noticeable differences in their tracking speed and accuracy. The P&O algorithm exhibits the poorest tracking performance, and its operating principle prevents it from reaching a stable operating point. This conclusion is evident from the P-D curve. The P&O algorithm is prone to becoming stuck at local extreme values, leading to a very low system efficiency. In comparison, both the PSO and HHO algorithms outperform the P&O algorithm in terms of tracking effectiveness. The PSO algorithm updates the position of all particles based on the optimal position in each iteration, but its repeated iterations lead to slow convergence. On the other hand, the HHO algorithm performs better than PSO, especially when dealing with output characteristics that become multi-modal due to changes in external conditions. The HHO algorithm's global search capabilities prove to be more effective.

Tables 6 and 7 summarize the grid-connected effects of various algorithms before and after irradiance changes. In conclusion, the simulation results verify that the HHO algorithm is superior in terms of speed, stability, and tracking accuracy compared with the P&O and PSO algorithms. The HHO algorithm shows great potential for practical applications in PV power-generation systems.

Table 6. Grid-connected effects of the different algorithms within 0–1 s.

Algorithms	P_{max}/W	Output Power/W	System Efficiency
P&O	1002.2	931.4	92.9%
PSO	1002.2	932.2	93.0%
HHO	1002.2	933.4	93.1%

Table 7. Grid-connected effects of the different algorithms within 1–2 s.

Algorithms	P_{max}'/W	Output Power/W	System Efficiency
P&O	806.4	544.5	67.5%
PSO	806.4	622.1	77.1%
HHO	806.4	661.2	82.0%

P_{max} and P_{max}' represent the theoretical maximum output power of the PV array before and after the change in irradiance, respectively, and system efficiency is the ratio of the output power to the maximum power of the PV array. Before the change in irradiance, the output power corresponding to the working points found by the three algorithms is similar, respectively 931.4 W, 932.2 W, and 933.4 W, because the output characteristic curve of the PV array before the change in irradiance is almost the same as the theoretical curve, showing single-peak characteristics. Furthermore, with regard to the PV array uneven lighting problem, the performance of the P&O algorithm differed greatly from the other two algorithms, with an output power of only 544.5 W, and an entire system efficiency of 67.5%. Obviously, the algorithm did not find the global optimal and only stopped at the local extreme point. The PSO algorithm still has a strong optimization ability, as after the irradiance changes, the algorithm could quickly restart and reach stability in about 0.4 s, and the final output power was 622.1 W, 14% higher than that from the P&O algorithm. Meanwhile, system efficiency also reached 77.1%, which is nearly 10% higher than that of the P&O algorithm. The output power of the HHO algorithm was the highest among the three algorithms, which was 661.2 W, and the system efficiency reached 82%, indicating that for the whole system, the HHO algorithm has a better optimization ability and a stronger ability to adapt and adjust to changes in external conditions.

6. Conclusions

MPPT technology is an important guarantee for the efficient operation of PV power systems. Compared with traditional algorithms and the PSO algorithm, the HHO algorithm's inclination toward exploring the search space makes it less susceptible to becoming trapped in the local optima, providing a significant advantage in photovoltaic power systems. The strengths and weaknesses of the commonly used MPPT algorithms were analyzed in this paper, and a new HHO-MPPT control scheme is proposed that applies the HHO algorithm to a PV power-generation system. This control method holds significant advantages in avoiding local optima and achieving rapid optimization.

The effectiveness of different MPPT algorithms, including the P&O, PSO, and HHO algorithms, was evaluated through simulations and verifications for a PV system. The experimental results show that the proposed HHO algorithm is 97.9% efficient under uniform irradiance, which is better than the other two compared algorithms. In addition, in terms of tracking speed, the proposed algorithm uses less than half of the tracking time of the PSO algorithm. Under uneven irradiance, the P&O algorithm falls into local peaks, and the efficiency of the PSO algorithm decreases dramatically. Not only does the HHO algorithm succeed in finding the global maximum-power point, but it also maintains a high tracking accuracy. Finally, a reliability test is conducted on the constructed single-phase full-bridge-inverter grid-connected system to verify the feasibility of the proposed algorithm in practical-use scenarios.

Author Contributions: Methodology, X.T., J.X., S.Z. and Z.X.; Software, B.C. and N.Z.; Validation, X.T., Z.Y. and K.W.; Formal analysis, N.Z.; Data curation, B.C.; Writing—original draft, X.T.; Writing—review and editing, J.X., S.Z., Z.X. and Z.Y.; Visualization, K.W.; Project administration, S.Z. All authors have read and agreed to the published version of the manuscript.

Funding: This work was supported by a Science and Technology Project of the State Grid Jiangxi Electric Power Co., Ltd. (NO:52182023000K).

Data Availability Statement: Data is contained within the article.

Conflicts of Interest: The authors declare that this study received funding from State Grid Jiangxi Electric Power Research Institute and State Grid Jiangxi Electric Power Co., Ltd. The funder had the following involvement with the study: A Novel Harris-Hawk-Optimization-Based Maximum-Power-Point-Tracking Control Strategy for a Grid-Connected PV Power-Generation System. The remaining authors declare that the research was conducted in the absence of any commercial or financial relationships that could be construed as a potential conflict of interest.

References

1. Yan, J.; Yang, Y.; Elia Campana, P.; He, J. City-level analysis of subsidy-free solar photovoltaic electricity price, profits and grid parity in China. *Nat. Energy* **2019**, *4*, 709–717. [CrossRef]
2. Dileep, G.; Singh, S.N. Maximum power point tracking of solar photovoltaic system using modified perturbation and observation method. *Renew. Sustain. Energy Rev.* **2015**, *50*, 109–129. [CrossRef]
3. Ahmed, J.; Salam, Z.; Kermadi, M.; Afrouzi, H.N.; Ashique, R.H. A skipping adaptive P&O MPPT for fast and efficient tracking under partial shading in PV arrays. *Int. Trans. Electr. Energy Syst.* **2021**, *31*, e13017.
4. Charaabi, A.; Zaidi, A.; Barambones, O.; Zanzouri, N. Implementation of adjustable variable step based backstepping control for the PV power plant. *Int. J. Electr. Power Energy Syst.* **2022**, *136*, 107682. [CrossRef]
5. Wang, Y.; Li, Y.; Ruan, X. Maximum power point tracking algorithm for photovoltaic array under partial shading based on current property. *Trans. China Electrotech. Soc.* **2016**, *31*, 201–210+218. [CrossRef]
6. Immad, S.; Saad, M.; Kok, T. Improved-Team-Game-Optimization-Algorithm-Based Solar MPPT with Fast Convergence Speed and Fast Response to Load Variations. *IEEE Trans. Ind. Electron.* **2020**, *68*, 7093–7103.
7. Immad, S.; Saad, M.; Kok, T. Improved Social Ski Driver-Based MPPT for Partial Shading Conditions Hybridized with Constant Voltage Method for Fast Response to Load Variations. *IEEE Trans. Sustain. Energy* **2021**, *12*, 2255–2267.
8. Zhao, Z.; Zhang, M.; Zhang, Z.; Wang, Y.; Cheng, R.; Guo, J.; Yang, P.; Lai, C.S.; Li, P.; Lai, L.L. Hierarchical Pigeon-Inspired Optimization-Based MPPT Method for Photovoltaic Systems Under Complex Partial Shading Conditions. *IEEE Trans. Ind. Electron.* **2022**, *69*, 10129–10143. [CrossRef]
9. Immad, S.; Saad, M.; Tey, K.T. Maximum Power Point Tracking Using Modified Butterfly Optimization Algorithm for Partial Shading, Uniform Shading, and Fast Varying Load Conditions. *IEEE Trans. Power Electron.* **2021**, *36*, 5569–5581.
10. Lian, K.L.; Jhang, J.H.; Tian, I.S. A maximum power point tracking method based on perturb-and-observe combined with particle swarm optimization. *IEEE J. Photovolt.* **2014**, *4*, 626–633. [CrossRef]
11. Ishaque, K.; Salam, Z. A deterministic particle swarm optimization maximum power point tracker for photovoltaic system under partial shading condition. *IEEE Trans. Ind. Electron.* **2012**, *60*, 3195–3206. [CrossRef]
12. Mao, M.; Zhang, L.; Yang, L.; Chong, B.; Huang, H.; Zhou, L. MPPT using modified salp swarm algorithm for multiple bidirectional PV-Ćuk converter system under partial shading and module mismatching. *Sol. Energy* **2020**, *209*, 334–349. [CrossRef]
13. Sara, A.; Hossein, I.; Shahrokh, F. Fast Artificial Neural Network Based Method for Estimation of the Global Maximum Power Point in Photovoltaic Systems. *IEEE Trans. Ind. Electron.* **2022**, *69*, 5879–5888.
14. Lin, D.; Li, X.; Ding, S.; Wen, H.; Du, Y.; Xiao, W. Self-Tuning MPPT Scheme Based on Reinforcement Learning and Beta Parameter in Photovoltaic Power Systems. *IEEE Trans. Power Electron.* **2021**, *36*, 13826–13838. [CrossRef]
15. Heidari, A.A.; Mirjalili, S.; Faris, H.; Aljarah, I.; Mafarja, M.; Chen, H. Harris hawks optimization: Algorithm and applications. *Future Gener. Comput. Syst.* **2019**, *97*, 849–872. [CrossRef]
16. Zhang, J.; Liu, Y.; Ding, K.; Feng, L.; Hamelmann, F.U.; Chen, X. Model Parameter Analysis of Cracked Photovoltaic Module under Outdoor Conditions. In Proceedings of the 2020 47th IEEE Photovoltaic Specialists Conference (PVSC), Calgary, AB, Canada, 15 June–21 August 2020; IEEE: Piscataway, NJ, USA, 2020; pp. 2509–2512.
17. Zhou, J.; Yu, Z.; Lu, Z.; Li, C.; Zhang, R. Study of photovoltaic cells engineering mathematical model. *IOP Conf. Ser. Mater. Sci. Eng.* **2016**, *157*, 012019. [CrossRef]
18. Syamala, L.; Sankar, D.; Makkar, S.E.; Jos, B.M.; Kallarackal, M. Hysteresis based quasi fixed frequency current control of single phase full bridge grid integrated voltage source inverter. *Energies* **2022**, *15*, 8112. [CrossRef]
19. Tsang, K.M.; Chan, W.L. Maximum power point tracking for PV systems under partial shading conditions using current sweeping. *Energy Convers. Manag.* **2015**, *93*, 249–258. [CrossRef]
20. Guo, K.; Cui, L.; Mao, M.; Zhou, L.; Zhang, Q. An improved gray wolf optimizer MPPT algorithm for PV system with BFBIC converter under partial shading. *IEEE Access* **2020**, *8*, 103476–103490. [CrossRef]